









LETTER | MARCH 01 2024

Giant microwave–optical Kerr nonlinearity via Rydberg excitons in cuprous oxide

Jon D. Pritchett ; Liam A. P. Gallagher ; Alistair Brewin; Horatio Q. X. Wong ; Wolfgang Langbein ; Stephen A. Lynch ; C. Stuart Adams ; Matthew P. A. Jones  



APL Photonics 9, 031303 (2024)

<https://doi.org/10.1063/5.0192710>



View
Online



Export
Citation



APL Machine Learning

2023 Papers with Best Practices in Data Sharing and Comprehensive Background

[Read Now](#)

 AIP
Publishing

Giant microwave–optical Kerr nonlinearity via Rydberg excitons in cuprous oxide

Cite as: APL Photon. 9, 031303 (2024); doi: 10.1063/5.0192710

Submitted: 20 December 2023 • Accepted: 7 February 2024 •

Published Online: 1 March 2024



Jon D. Pritchett,¹  Liam A. P. Gallagher,¹  Alistair Brewin,¹ Horatio Q. X. Wong,¹  Wolfgang Langbein,² 
 Stephen A. Lynch,²  C. Stuart Adams,¹  and Matthew P. A. Jones^{1,a)} 

AFFILIATIONS

¹Department of Physics, Durham University, Durham DH1 3LE, United Kingdom

²School of Physics and Astronomy, Cardiff University, Cardiff CF24 3AA, United Kingdom

^{a)}Author to whom correspondence should be addressed: m.p.a.jones@durham.ac.uk

ABSTRACT

Microwave–optical conversion is key to future networks of quantum devices, such as those based on superconducting technology. Conversion at the single quantum level requires strong nonlinearity, high bandwidth, and compatibility with a millikelvin environment. A large nonlinearity is observed in Rydberg atoms, but combining atomic gases with dilution refrigerators is technically challenging. Here, we demonstrate a strong microwave–optical nonlinearity in a cryogenic, solid-state system by exploiting Rydberg states of excitons in Cu₂O. We measure a microwave–optical cross-Kerr coefficient of $B_0 = 0.022 \pm 0.008 \text{ m V}^{-2}$ at 4 K, which is several orders of magnitude larger than other solid-state systems. The results are in quantitative agreement with a nonlinear susceptibility model based on the giant microwave dipole moment between nearby excitonic states. Our results highlight the potential of Rydberg excitons for nonlinear optics and form the basis for a microwave–optical frequency converter based on Cu₂O.

© 2024 Author(s). All article content, except where otherwise noted, is licensed under a Creative Commons Attribution (CC BY) license (<http://creativecommons.org/licenses/by/4.0/>). <https://doi.org/10.1063/5.0192710>

Superconducting microwave devices play a key role in quantum computation.¹ To eliminate thermal noise, these devices must be cooled to $T \approx 10 \text{ mK}$, a requirement that makes direct quantum networking impractical over distances larger than $\sim 1 \text{ m}$.² Microwave–optical (MO) conversion is, therefore, a critical enabling technology,^{3–5} with current approaches, including electro-optics,^{6,7} rare-earth ions,⁸ optomechanical systems,^{9,10} and quantum dot molecules.¹¹ Very strong nonlinearity can be achieved by exploiting the large microwave dipole moment associated with highly excited atomic Rydberg states,^{12,13} leading to the largest observed cross-Kerr effect of any material.¹⁴ However, interfacing Rydberg atoms with planar superconducting quantum devices in a millikelvin environment is an outstanding challenge, and coupling has so far been achieved only at much higher temperatures.^{15–18}

In this Letter, we combine the advantages of atomic Rydberg states (giant nonlinearity) and the solid state (millikelvin compatibility^{19,20}) by using Rydberg states of excitons in the bulk semiconductor Cu₂O²¹ (Fig. 1). Excitons are optically excited bound states of an electron and a hole, with an internal structure that resembles a hydrogen atom. In Cu₂O, the resulting Rydberg series of

excitonic states has been measured up to principal quantum number $n = 30$ at $T \approx 40 \text{ mK}$.²⁰ Transitions between neighboring states of opposite parity are located in the microwave spectral region. The associated dipole moment scales as $d \propto n^2$, reaching $180e \text{ nm}$ at $n = 11$, which is more than 30 times larger than in quantum dot molecules.¹¹ Thus, Rydberg excitons in Cu₂O provide a unique platform for MO coupling in the solid-state,²² with recent experiments demonstrating microwave control of the linear and nonlinear optical response.²³ Here, we extend this work to a measurement of the optical phase shift induced by the presence of a microwave field, characterized by the microwave–optical Kerr coefficient B_0 ,

$$B_0 = \frac{\Delta\phi}{2\pi L |\mathcal{E}_{\text{MW}}|^2}, \quad (1)$$

where $\Delta\phi$ is the optical phase shift induced by the microwave field, L is the length of the material, and \mathcal{E}_{MW} is the amplitude of the applied microwave field.

A schematic of the experiment is shown in Fig. 1. A thin slab of Cu₂O ($55 \pm 10 \mu\text{m}$) is mounted between the conductors of a

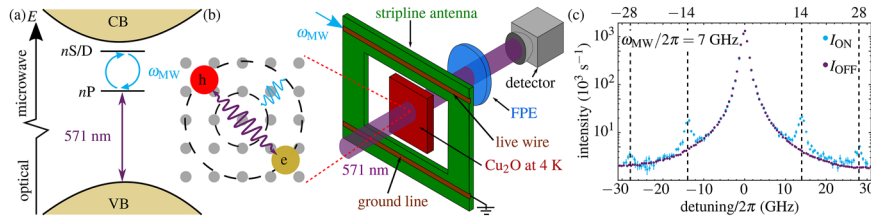


FIG. 1. (a) Excitons are created in state nP via laser excitation at $\lambda \approx 571$ nm. A microwave field at frequency ω_{MW} couples odd- and even-parity exciton states. The exciton wavefunction spans many lattice sites, giving rise to a large dipole moment. (b) Excitons are created in a thin slab of Cu_2O located between the conductors of a microwave strip line. The transmitted light is filtered with a Fabry-Pérot etalon (FPE) and sent to a detector. (c) Example spectrum of the transmitted light for $E = hc/\lambda = 2.170\,927$ eV and $\mathcal{E}_{MW} = 640$ V/m, showing an array of sidebands at $\pm 2\omega_{MW}/(2\pi)$ and $\pm 4\omega_{MW}/(2\pi)$ when microwaves are applied (I_{ON}).

microwave strip line and cooled to $T = 4$ K. Excitons in a quantum state nP (where P denotes the orbital angular momentum $l = 1$) were excited from the ground state (valence band) using a single-frequency laser at wavelength $\lambda \approx 571$ nm. A microwave field at angular frequency $\omega_{MW} = 2\pi \times 7$ GHz couples nP states to the nearby states of opposite parity (e.g., $n'S$ and $n'D$, where S and D indicate $l = 0$ and $l = 2$). The spectrum of the transmitted laser light was resolved using a scanning Fabry-Pérot etalon. Further experimental details are provided in Appendix A. Applying the microwave field leads to a change in transmission at the laser frequency $\omega_L = 2\pi c/\lambda$ and the appearance of sidebands at frequencies $\omega_L \pm 2\omega_{MW}$ on the light transmitted through the sample [Fig. 1(c)] that are indicative of a cross-Kerr nonlinearity. As the microwave field amplitude is increased further, higher order sidebands (e.g., $\omega_L \pm 4\omega_{MW}$) become visible.

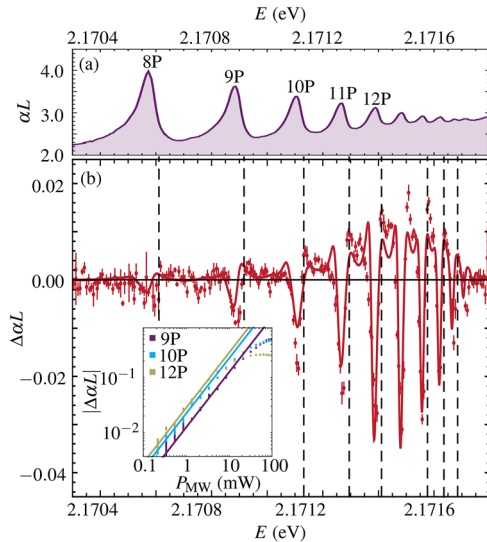


FIG. 2. (a) Rydberg series of exciton absorption lines. (b) Measured (red points) and predicted (solid line) change in absorption, $\Delta\alpha L$ at $\mathcal{E}_{MW} = 38$ V/m. The dashed lines indicate the zero crossings used to extract the Kerr coefficient. The inset shows $|\Delta\alpha L|$ vs microwave power P_{MW} at the $n = 9, 10, 12P$ resonances. The solid lines are fits to the linear region.

The optical absorption spectrum close to the bandgap is shown in Fig. 2(a). Peaks corresponding to nP excitonic states are visible up to $n = 16$, limited by a combination of temperature and sample quality. As Cu_2O is centrosymmetric, the MO coupling is absent from the ground-state symmetry but is created by the Rydberg excitons, as shown in Fig. 2(b), which plots the spectrum of the microwave-induced change in absorption $\Delta\alpha L$. Each exciton resonance shows decreased absorption on-resonance and increased absorption on each side at the location of the nS and nD states. In contrast to Rydberg atoms, a response is observed over a wide range of n , even for a single microwave frequency. This is due to non-radiative broadening of the exciton lines, which means that the microwave field is near-resonant with many transitions simultaneously. The same effect results in a broad microwave frequency dependence (see Appendix A and Ref. 23). $|\Delta\alpha L|$ increases with n up to $n = 13$ before decreasing toward the band edge. As shown in the inset of Fig. 2(b), $|\Delta\alpha L|$ increases linearly with the microwave power as expected for a Kerr nonlinearity, before saturating at a value that depends on n . Saturation occurs due to multi-photon processes and is accompanied by the appearance of the higher-order (fourth-order) sidebands in Fig. 1(c). For the remainder of this paper, we consider only the linear regime.

The MO Kerr nonlinearity can be described in terms of the dielectric polarization at the laser frequency,

$$\mathcal{P}(\omega_L) = \epsilon_0 \left(\chi^{(1)}(\omega_L) \mathcal{E}_L + \chi^{(3)}(\omega_L) \mathcal{E}_L \mathcal{E}_{MW} \mathcal{E}_{MW} + \dots \right),$$

where $\chi^{(1)}$ and $\chi^{(3)}$ are the linear and Kerr nonlinear susceptibilities, respectively. Experimentally, we observe that the nonlinearity depends very weakly on the laser and microwave polarizations, and so a scalar treatment is used. We obtain an expression for $\chi^{(3)}$ by treating the exciton states as hydrogen-like.²³ $\Delta\alpha$ is related to the imaginary part of the susceptibility,

$$\frac{\Delta\alpha c}{\omega_L |\mathcal{E}_{MW}|^2} = \text{Im} \left(\chi^{(3)}(\omega_L) \right) = \text{Im} \left(\sum_{n,n',l',n'',\pm} \chi_{nPn'l'n''P}^{(3)}(\omega_L) \right).$$

Each term in the sum is given by

$$\chi_{nPn'l'n''P}^{(3)}(\omega_L) = \frac{N_d}{8\epsilon_0 \hbar^3} \frac{D^{VB \rightarrow nP} a^{nP \rightarrow n'l'} a^{n'l' \rightarrow n''P} D^{n''P \rightarrow VB}}{(\delta_{nP} - i\Gamma_{nP})(\delta_{n'l'}^{\pm\omega_{MW}} - i\Gamma_{n'l'}) (\delta_{n''P} - i\Gamma_{n''P})}, \quad (2)$$

where N_d is the effective density of exciton states, D are the effective matrix elements for transitions from the valence band to the P states, d are the dipole matrix elements for transitions between exciton states, Γ are the exciton linewidths, and δ are detunings, given by $\delta_{nP} = \omega_{nP} - \omega_L$ and $\delta_{n'l'}^{\pm\omega_{MW}} = \omega_{n'l'} - (\omega_L \pm \omega_{MW})$. Crucially, all these parameters are either known theoretically or can be derived from the analysis of data without a microwave field applied (see Appendix B), enabling the use of Eq. (2) for quantitative predictions of the nonlinear response.

The predicted $\Delta\alpha$ is compared with the data in Fig. 2(b). The only adjustable parameter is the amplitude of the microwave electric field \mathcal{E}_{MW} . The prediction is in excellent agreement with the data over the full range of n . Similar levels of agreement are observed up to field amplitudes of 60 V/m, above which saturation occurs.

We exploit the quantitative agreement Fig. 2(b) to calibrate the microwave electric field amplitude \mathcal{E}_{MW} . The model was fitted to the change in absorption over a range of applied microwave powers. From these fits, we obtain a calibration between electric field amplitude and applied microwave power of 43 ± 3 (V/m)/mW^{1/2}, in reasonable agreement with a value of 70 (V/m)/mW^{1/2} obtained from a finite-element simulation of the antenna that excludes connection losses.²³ More details are given in Appendix C.

Once the electric field is known, the real part of the susceptibility can be used to make a quantitative prediction of the microwave-optical Kerr coefficient,

$$B_0 = \frac{\omega_L}{4\eta\pi c} \text{Re}(\chi^{(3)}(\omega_L)),$$

where $\eta = 2.8$ is the optical refractive index. The predicted values of B_0 are shown in Fig. 3(a).

To independently measure B_0 , we make use of the zero-crossings in Fig. 2. At these points $\Delta\alpha = 0$, the imaginary part of the susceptibility is zero, and sidebands are generated via phase modulation only. By using the conventional expansion of a phase-modulated wave in terms of Bessel functions, it can be shown that the ratio of the intensity of the sidebands to the carrier is $I_{SB}/I_C = |J_1(\Delta\phi)|^2$, where J_1 is the first-order Bessel function of the first

kind. Thus, the microwave-induced phase shift $\Delta\phi$ can be directly extracted from spectra like Fig. 1(c).

The variation in $\Delta\phi$ with $|\mathcal{E}_{MW}|^2$ is shown for two zero-crossings in Fig. 3(b). As expected, the phase shift increases linearly in the Kerr regime, before saturating. The Kerr coefficient is obtained from the gradient in the linear regime using Eq. (1) and the electric field calibration described previously.

As shown in Fig. 3(a), the measured Kerr coefficient is in agreement with the prediction. We emphasize that the phase shift measurement does not depend on the model for $\chi^{(3)}$ [Eq. (2)] and its input parameters; these affect the measured value of B_0 only through the field calibration. The dominant experimental uncertainties come from the electric field calibration and the thickness of the sample. The analysis also assumes that $\chi^{(3)}(\omega_L \pm 2\omega_{MW}) = \chi^{(3)}(\omega_L)$, which is not strictly true due to the strong energy dependence near resonance. An indication that this assumption does not fully hold is the asymmetry in the red and blue sideband amplitudes in Fig. 3. We, therefore, include the difference between the red and blue values as part of the uncertainty in B_0 and present the average value. The analytic expressions for $\chi^{(3)}(\omega_L \pm 2\omega_{MW})$ are provided in Appendix D.

Our highest measured value of $B_0 = 0.022 \pm 0.008$ V m⁻² at $n = 12$ is compared to other low-frequency (DC) Kerr coefficients in Table I. Our measured Kerr coefficient is extremely large due to a combination of the underlying resonant nature of the nonlinearity and the large dipole moment. The other values in Table I were measured far from resonance—a key feature of Cu₂O is that a much larger but still broadband response can be obtained via multiple resonances. Cu₂O also has the highest absorption coefficient among the materials in Table I. An alternative figure of merit is the phase shift per unit absorption length and microwave intensity, described by the ratio $\mathcal{F} = B_0/\alpha$, where α is the linear absorption coefficient. Here, Cu₂O has the largest \mathcal{F} , with only Rydberg atoms in Rb vapor being comparable, highlighting the importance of Rydberg physics in the solid state.

Despite the large values of B_0 and \mathcal{F} , the maximum phase shift remained limited to around 0.1 rad as shown in Fig. 3(b). This is due to a combination of the saturation of the phase shift at high electric fields and the high background absorption, which together limit the maximum phase shift that can be measured. The saturation is a consequence of the extremely strong nonlinearity and corresponds to the emergence of higher order terms (e.g., $\chi^{(5)}$) in the

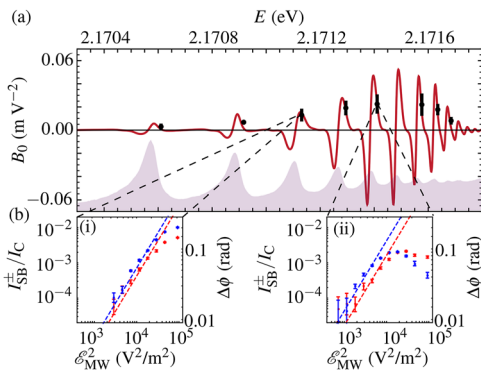


FIG. 3. (a) Predicted (solid line) and measured (points) Kerr coefficient vs excitation energy E . The shaded area shows the exciton spectrum from $n = 8$ upward for reference. (b) I_{SB}/I_C vs \mathcal{E}_{MW} for positive frequency (blue) and negative frequency (red) sidebands. The right-hand side axis gives the corresponding phase shift.

TABLE I. Comparison of Kerr (B_0) and absorption (α) coefficients, and their ratio $\mathcal{F} = B_0/\alpha$ for various materials. For nitrobenzene, glass and Cu₂O $\lambda = 570$ nm; for PMN-PT (a transparent ceramic) and GO-LC (graphene oxide liquid crystals) $\lambda = 633$ nm; Rb vapor $\lambda = 780$ nm.

Material	B_0 (m V ⁻²)	α (m ⁻¹)	\mathcal{F} (m ² V ⁻²)
Glass ²⁴	10 ⁻¹⁴	10 ⁻¹	10 ⁻¹³
Nitrobenzene ^{24,25}	10 ⁻¹²	10 ⁻¹	10 ⁻¹¹
PMN-PT ²⁶	10 ⁻⁷	10 ²	10 ⁻⁹
GO-LC ^{27,28}	10 ⁻⁶	10 ³	10 ⁻⁹
Rb vapor ^{14,29}	10 ⁻⁶	10 ¹	10 ⁻⁷
Cu ₂ O	10 ⁻²	10 ⁴	10 ⁻⁶

susceptibility. In fact, the experiment enters the ultra-strong driving regime, where the coupling strength $\Omega_{\text{MW}} = d\mathcal{E}_{\text{MW}}/\hbar \gg \omega_{\text{MW}}, \Gamma$. Microwave–optical conversion still occurs in this regime, but it is no longer given by a simple Kerr effect. A reduction in absorption would enable the use of thicker samples, resulting in larger phase shifts. The absorption is dominated by phonon-assisted processes that do not involve Rydberg states, and which are unaffected by the microwave field.³⁰ At $n = 11$, 80% of the absorption coefficient is due to the background. As in atomic Rydberg gases, the background may be reduced by nonlinear spectroscopy techniques, such as second harmonic generation^{31,32} or electromagnetically induced transparency,^{29,33} or by exploiting Rydberg exciton–polaritons.³⁴

Finally, we discuss our results in the context of MO conversion, where the standard figures of merit are bandwidth and conversion efficiency.³ Large bandwidth is the major advantage of Cu_2O ; our model predicts that the Kerr coefficient varies by less than a factor of two over the entire range $\omega_{\text{MW}}/2\pi = 1 - 20$ GHz (see Appendix A). For comparison, most platforms have a bandwidth of less than 10 MHz³ with quantum dot molecules achieving 100s of MHz.¹¹ Conversion efficiency is critically dependent on the optimization of the device parameters (e.g., mode volume), which we did not study here. Instead, we compare the intrinsic strength of the nonlinearity with lithium niobate (LN), which can also provide a broadband response.^{35–37} The refractive index change in a Kerr medium becomes larger than that in a linear electro-optic medium, such as LN above a critical field given by $\mathcal{E}_{\text{crit}} = c\eta_{\text{EO}}^3 r / (2\omega_L B_0)$, where r_{EO} and η_{EO} are the electro-optic coefficient and refractive index of the linear medium, respectively.³⁵ Comparing Cu_2O with LN, we find $E_{\text{crit}} = 0.01 \text{ V m}^{-1}$, which is 20 times lower than the rms vacuum field in typical superconducting quantum circuits.³⁸ Given the nonlinearity in Cu_2O should improve as the temperature is reduced (due to increased exciton oscillator strength¹⁹ and the accessibility of higher n^{20}), Cu_2O appears to be a promising candidate to achieve a high-bandwidth, efficient microwave–optical conversion.

In conclusion, we have demonstrated that the strong microwave–optical nonlinearity observed in atomic gases can be realized in a cryogenic, solid-state setting using Rydberg excitons in Cu_2O . The experimentally measured Kerr coefficient $B_0 = 0.022 \pm 0.008 \text{ m V}^{-2}$ is four orders of magnitude larger than other solid-state platforms, with only Rydberg atoms being comparable. The observations are in agreement with a model based on the conventional hydrogen-like theory of Wannier–Mott excitons, enabling the quantitative design of future devices that exploit the giant Kerr effect; in addition, we highlight that the effect is visible at relatively low n , meaning that synthetic materials could be utilized.^{39–41} Our work complements efforts to prepare quantum states of light using Rydberg-mediated interactions in Cu_2O ^{42–45} and opens a potential route to microwave–optical conversion in the quantum regime.

ACKNOWLEDGMENTS

We thank I. Chaplin and S. Edwards for preparing samples and V. Walther for calculating the dipole matrix elements. This work was supported by the Engineering and Physical Sciences Research Council (EPSRC), United Kingdom, through research Grant Nos. EP/P011470/1, EP/P012000/1, EP/X038556/1, and EP/X03853X/1.

AUTHOR DECLARATIONS

Conflict of Interest

The authors have no conflicts to disclose.

Author Contributions

J.D. and L.A.P.G. contributed equally to this work.

Jon D. Pritchett: Formal analysis (equal); Investigation (lead); Methodology (equal); Writing – review & editing (equal). **Liam A. P. Gallagher:** Formal analysis (equal); Investigation (supporting); Methodology (equal); Visualization (lead); Writing – original draft (lead); Writing – review & editing (equal). **Alistair Brewin:** Formal analysis (equal); Writing – review & editing (equal). **Horatio Q. X. Wong:** Formal analysis (supporting); Investigation (supporting); Writing – review & editing (supporting). **Wolfgang Langbein:** Methodology (equal); Writing – review & editing (equal). **Stephen A. Lynch:** Methodology (supporting); Writing – review & editing (equal). **C. Stuart Adams:** Conceptualization (supporting); Methodology (supporting); Supervision (supporting); Writing – review & editing (supporting). **Matthew P. A. Jones:** Conceptualization (lead); Methodology (lead); Supervision (lead); Writing – original draft (equal); Writing – review & editing (lead).

DATA AVAILABILITY

The data that support the findings of this study are openly available at <https://doi.org/10.15128/r27d278t10x>.

APPENDIX A: EXPERIMENTAL DETAILS

The Cu_2O sample was prepared from a natural gemstone (Tsumeb mine) using the procedure detailed in Ref. 39 and glued to a CaF_2 window. The light had an incident intensity of $20 \mu\text{W}/\text{mm}^2$, propagated along the [111] crystallographic axis, and was linearly polarized. Finite element analysis showed that the microwave electric field was aligned in the plane of the sample and orthogonal to strip line. $\Delta\alpha$ was observed to depend very weakly on the angle between microwave and optical electric fields with a less than 10% difference observed when varying the angle by $\pi/2$.⁴⁶ No microwave-induced change in the polarization of the transmitted light was observed within the experimental uncertainty. The etalon had a free spectral range of 60.1 ± 0.2 GHz and a finesse of 44.5 ± 0.7 and was temperature-tuned. The carrier and sideband amplitudes were extracted by fitting the Lorentzian response function of the etalon to spectra like those in Fig. 1(c).

As stated in the text, the nonlinear response is very broadband. The predicted Kerr coefficient as a function of microwave frequency is shown in Fig. 4 over the range 1–20 GHz. Measurements at multiple frequencies²³ are challenging in our current setup due to parasitic resonances in the cryostat. We, therefore, fixed $\omega_{\text{MW}} = 2\pi \times 7$ GHz to give good resolution of the sidebands while remaining in the relevant range for superconducting quantum circuits.

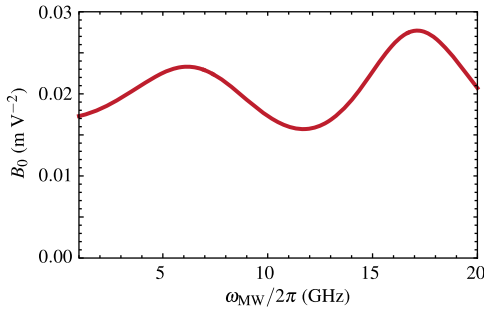


FIG. 4. Predicted dependence of the Kerr coefficient B_0 on microwave frequency ω_{MW} at excitation energy $E = 2.171\,411\text{ eV}$.

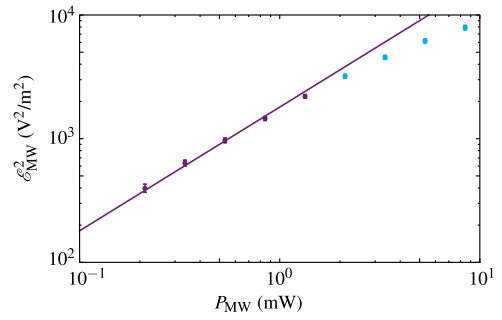


FIG. 5. Square of the fitted microwave electric field strength \mathcal{E}_{MW} vs microwave power applied at the input port of the strip line (output terminated at $50\ \Omega$) P_{MW} . By fitting the region where the model is valid (purple points) with a linear trend (purple line), the electric field calibration is extracted.

APPENDIX B: PARAMETERS FOR MODEL

Here, we give details of the parameters in the susceptibility model [Eq. (2)]. States from $n = 5\text{--}17$ and $l = 0\text{--}2$ are included in the model.

Matrix elements for transitions between exciton states, d , were calculated using a spinless hydrogen-like model³³ for the exciton states, with quantum defects obtained from dispersion relations for the electron and the hole.⁴⁷

The widths and energies were extracted from experimental absorption spectra without microwaves. The product $N_d|D|^2$ was determined from the area of the exciton peaks in the absorption spectra without microwaves.

The values for the energy and width of the S and D states were extracted from Ref. 32. In the two-photon experiments only, states up to $n = 12$ were observed, and so extrapolation was used to extend the range of n beyond that available from these experiments. The energies were extrapolated using a quantum defect model,

$$E_{nl} = E_g - \frac{R_X}{(n - \delta_l)^2}, \quad (\text{B1})$$

where R_X is the excitonic Rydberg energy and δ_l is the quantum defect.

The widths of the P states were fitted using the following equation:

$$\Gamma_{nP} = \frac{\Gamma}{n^3} + \Gamma_0, \quad (\text{B2})$$

where Γ_0 is a constant offset attributed to an inhomogeneous broadening due to charges and defects in the material.⁴⁸ For the S and D widths, the Γ_0 was fixed to the value fitted from the P state trend and the high n states were extrapolated.

APPENDIX C: ELECTRIC FIELD CALIBRATION

Here, we provide further details of the electric field calibration. By fitting the model to the change in absorption [see Fig. 2(b) for an example] at different applied microwave powers P_{MW} , it is possible to extract the calibration between the externally applied power and \mathcal{E}_{MW} . The result is shown in Fig. 5. As expected, the relation between $|\mathcal{E}_{\text{MW}}|^2$ and power is linear at low electric fields, before a deviation occurs as the susceptibility model breaks down due to the

higher-order processes discussed in the text. The quantitative agreement between the model and the data illustrated in Fig. 2(b) holds for all powers within the linear range.

Fitting the linear region in Fig. 5 (purple points) gives a value of $43 \pm 3\text{ (V/m)/mW}^{1/2}$. A simulation of the strip line antenna and the surrounding environment using a commercial finite element analysis software package (see Ref. 23) yields a value of $70\text{ (V/m)/mW}^{1/2}$. We consider that these values are in reasonable agreement, especially since no connection losses were included in the simulation. Using the simulated value for the calibration would reduce the measured Kerr coefficient by a factor of ~ 3 , which remains the orders of magnitude larger than in other solid-state systems.

APPENDIX D: SIDEBAND SUSCEPTIBILITY

The nonlinear susceptibility at the frequency of the red and blue sidebands is

$$\begin{aligned} \chi_{nPn'l'n''p}^{(3)}(\omega_L \pm 2\omega_{\text{MW}}) \\ = \frac{N_d}{2\epsilon_0\hbar^3} \frac{D^{\text{VB} \rightarrow nP} d^{nP \rightarrow n'l'} d^{n'l' \rightarrow n''P} D^{n''P \rightarrow \text{VB}}}{(\delta_{nP} - i\Gamma_{nP})(\delta_{n'l'}^{\pm\omega_{\text{MW}}} - i\Gamma_{n'l'}) (\delta_{n''P}^{\pm 2\omega_{\text{MW}}} - i\Gamma_{n''P})}. \end{aligned} \quad (\text{D1})$$

The only difference between this and Eq. (2) is the detuning in the third term on the denominator, which is given by $\delta_{n''P}^{\pm 2\omega_{\text{MW}}} = \omega_{n''P} - (\omega_L \pm 2\omega_{\text{MW}})$. In principle, it is possible to derive the sideband amplitude by using these susceptibilities as source terms. However, this calculation is strongly dependent on the unknown relative phase of each term in the summation.³²

REFERENCES

- M. Kjaergaard, M. E. Schwartz, J. Braumüller, P. Krantz, J. I.-J. Wang, S. Gustavsson, and W. D. Oliver, “Superconducting qubits: Current state of play,” *Annu. Rev. Condens. Matter Phys.* **11**, 369–395 (2020).
- S. Storz, J. Schär, A. Kulikov, P. Magnard, P. Kurpiers, J. Lütolf, T. Walter, A. Copetudo, K. Reuer, A. Akin, J.-C. Besse, M. Gabureac, G. J. Norris, A. Rosario, F. Martin, J. Martinez, W. Amaya, M. W. Mitchell, C. Abellan, J.-D. Bancal,

- N. Sangouard, B. Royer, A. Blais, and A. Wallraff, "Loophole-free Bell inequality violation with superconducting circuits," *Nature* **617**, 265–270 (2023).
- ³N. Lauk, N. Sinclair, S. Barzanjeh, J. P. Covey, M. Saffman, M. Spiropulu, and C. Simon, "Perspectives on quantum transduction," *Quantum Sci. Technol.* **5**, 020501 (2020).
- ⁴N. J. Lambert, A. Rueda, F. Sedlmeir, and H. G. L. Schwefel, "Coherent conversion between microwave and optical photons—An overview of physical implementations," *Adv. Quantum Technol.* **3**, 1900077 (2020).
- ⁵X. Han, W. Fu, C.-L. Zou, L. Jiang, and H. X. Tang, "Microwave-optical quantum frequency conversion," *Optica* **8**, 1050–1064 (2021).
- ⁶C. Wang, I. Gonin, A. Grassellino, S. Kazakov, A. Romanenko, V. P. Yakovlev, and S. Zorzetti, "High-efficiency microwave-optical quantum transduction based on a cavity electro-optic superconducting system with long coherence time," *npj Quantum Inf.* **8**, 149 (2022).
- ⁷R. D. Delaney, M. D. Urmey, S. Mittal, B. M. Brubaker, J. M. Kindem, P. S. Burns, C. A. Regal, and K. W. Lehnert, "Superconducting-qubit readout via low-backaction electro-optic transduction," *Nature* **606**, 489–493 (2022).
- ⁸J. G. Bartholomew, J. Rochman, T. Xie, J. M. Kindem, A. Ruskuc, I. Craiciu, M. Lei, and A. Faraon, "On-chip coherent microwave-to-optical transduction mediated by ytterbium in YVO₄," *Nat. Commun.* **11**, 3266 (2020).
- ⁹M. Mirhosseini, A. Sipahigil, M. Kalaei, and O. Painter, "Superconducting qubit to optical photon transduction," *Nature* **588**, 599–603 (2020).
- ¹⁰S. Hönl, Y. Popoff, D. Caimi, A. Beccari, T. J. Kippenberg, and P. Seidler, "Microwave-to-optical conversion with a gallium phosphide photonic crystal cavity," *Nat. Commun.* **13**, 2065 (2022).
- ¹¹Y. Tsuchimoto, Z. Sun, E. Togan, S. Fält, W. Wegscheider, A. Wallraff, K. Ensslin, A. m. c. Imamoglu, and M. Kroner, "Large-bandwidth transduction between an optical single quantum dot molecule and a superconducting resonator," *PRX Quantum* **3**, 030336 (2022).
- ¹²J. Han, T. Vogt, C. Gross, D. Jaksch, M. Kiffner, and W. Li, "Coherent microwave-to-optical conversion via six-wave mixing in Rydberg atoms," *Phys. Rev. Lett.* **120**, 093201 (2018).
- ¹³S. Borówka, U. Pylypenko, M. Mazelanik, and M. Parniak, "Continuous wideband microwave-to-optical converter based on room-temperature Rydberg atoms," *Nat. Photonics* **18**, 32–38 (2024).
- ¹⁴A. K. Mohapatra, M. G. Bason, B. Butscher, K. J. Weatherill, and C. S. Adams, "A giant electro-optic effect using polarizable dark states," *Nat. Phys.* **4**, 890–894 (2008).
- ¹⁵S. D. Hogan, J. A. Agner, F. Merkt, T. Thiele, S. Filipp, and A. Wallraff, "Driving Rydberg-Rydberg transitions from a coplanar microwave waveguide," *Phys. Rev. Lett.* **108**, 063004 (2012).
- ¹⁶C. Hermann-Avigliano, R. C. Teixeira, T. L. Nguyen, T. Cantat-Moltrecht, G. Nogues, I. Dotsenko, S. Gleyzes, J. M. Raimond, S. Haroche, and M. Brune, "Long coherence times for Rydberg qubits on a superconducting atom chip," *Phys. Rev. A* **90**, 040502 (2014).
- ¹⁷A. A. Morgan and S. D. Hogan, "Coupling Rydberg atoms to microwave fields in a superconducting coplanar waveguide resonator," *Phys. Rev. Lett.* **124**, 193604 (2020).
- ¹⁸M. Kaiser, C. Glaser, L. Y. Ley, J. Grimmel, H. Hattermann, D. Bothner, D. Koelle, R. Kleiner, D. Petrosyan, A. Günther, and J. Fortágh, "Cavity-driven Rabi oscillations between Rydberg states of atoms trapped on a superconducting atom chip," *Phys. Rev. Res.* **4**, 013207 (2022).
- ¹⁹J. Heckötter, D. Janas, R. Schwartz, M. Aßmann, and M. Bayer, "Experimental limitation in extending the exciton series in Cu₂O towards higher principal quantum numbers," *Phys. Rev. B* **101**, 235207 (2020).
- ²⁰M. A. M. Versteegh, S. Steinhauer, J. Bajo, T. Lettner, A. Soro, A. Romanova, S. Gyger, L. Schweickert, A. Mysyrowicz, and V. Zwiller, "Giant Rydberg excitons in Cu₂O probed by photoluminescence excitation spectroscopy," *Phys. Rev. B* **104**, 245206 (2021).
- ²¹T. Kazimierzczuk, D. Fröhlich, S. Scheel, H. Stolz, and M. Bayer, "Giant Rydberg excitons in the copper oxide Cu₂O," *Nature* **514**, 343–347 (2014).
- ²²D. Ziemkiewicz and S. Zielińska-Raczyńska, "Optical-to-microwave frequency conversion with Rydberg excitons," *Phys. Rev. B* **107**, 195303 (2023).
- ²³L. A. P. Gallagher, J. P. Rogers, J. D. Pritchett, R. A. Mistry, D. Pizzey, C. S. Adams, M. P. A. Jones, P. Grünwald, V. Walther, C. Hodges, W. Langbein, and S. A. Lynch, "Microwave-optical coupling via Rydberg excitons in cuprous oxide," *Phys. Rev. Res.* **4**, 013031 (2022).
- ²⁴M. J. Weber, *Handbook of Optical Materials* (CRC Press, 2002).
- ²⁵M. H. Cabrera, O. A. Marciano, A. J. Ojeda *et al.*, "Absorption spectra of nitrobenzene measured with incoherent white-light excitation," *AIP Conf. Proc.* **992**, 1183–1188 (2008).
- ²⁶W. Ruan, G. Li, J. Zeng, J. Bian, L. S. Kamzina, H. Zeng, L. Zheng, and A. Ding, "Large electro-optic effect in La-doped 0.75Pb(Mg_{1/3}Nb_{2/3})O₃–0.25PbTiO₃ transparent ceramic by two-stage sintering," *J. Am. Ceram. Soc.* **93**, 2128–2131 (2010).
- ²⁷T.-Z. Shen, S.-H. Hong, and J.-K. Song, "Electro-optical switching of graphene oxide liquid crystals with an extremely large Kerr coefficient," *Nat. Mater.* **13**, 394–399 (2014).
- ²⁸V. H. Pham, T. V. Cuong, S. H. Hur, E. Oh, E. J. Kim, E. W. Shin, and J. S. Chung, "Chemical functionalization of graphene sheets by solvothermal reduction of a graphene oxide suspension in N-methyl-2-pyrrolidone," *J. Mater. Chem.* **21**, 3371–3377 (2011).
- ²⁹A. K. Mohapatra, T. R. Jackson, and C. S. Adams, "Coherent optical detection of highly excited Rydberg states using electromagnetically induced transparency," *Phys. Rev. Lett.* **98**, 113003 (2007).
- ³⁰P. W. Baumeister, "Optical absorption of cuprous oxide," *Phys. Rev.* **121**, 359–362 (1961).
- ³¹J. Mund, D. Fröhlich, D. R. Yakovlev, and M. Bayer, "High-resolution second harmonic generation spectroscopy with femtosecond laser pulses on excitons in Cu₂O," *Phys. Rev. B* **98**, 085203 (2018).
- ³²J. P. Rogers, L. A. P. Gallagher, D. Pizzey, J. D. Pritchett, C. S. Adams, M. P. A. Jones, C. Hodges, W. Langbein, and S. A. Lynch, "High-resolution nanosecond spectroscopy of even-parity Rydberg excitons in Cu₂O," *Phys. Rev. B* **105**, 115206 (2022).
- ³³V. Walther, P. Grünwald, and T. Pohl, "Controlling exciton-phonon interactions via electromagnetically induced transparency," *Phys. Rev. Lett.* **125**, 173601 (2020).
- ³⁴K. Orfanakis, S. K. Rajendran, V. Walther, T. Volz, T. Pohl, and H. Ohadi, "Rydberg exciton-polaritons in a Cu₂O microcavity," *Nat. Mater.* **21**, 767–772 (2022).
- ³⁵G. Chen, N. Li, J. D. Ng, H.-L. Lin, Y. Zhou, Y. H. Fu, L. Y. T. Lee, Y. Yu, A.-Q. Liu, and A. J. Danner, "Advances in lithium niobate photonics: Development status and perspectives," *Adv. Photonics* **4**, 034003 (2022).
- ³⁶T. P. McKenna, J. D. Witmer, R. N. Patel, W. Jiang, R. Van Laer, P. Arrangoiz-Arriola, E. A. Wollack, J. F. Herrmann, and A. H. Safavi-Naeini, "Cryogenic microwave-to-optical conversion using a triply resonant lithium-niobate-on-sapphire transducer," *Optica* **7**, 1737–1745 (2020).
- ³⁷Y. Xu, A. A. Sayem, L. Fan, C.-L. Zou, S. Wang, R. Cheng, W. Fu, L. Yang, M. Xu, and H. X. Tang, "Bidirectional interconversion of microwave and light with thin-film lithium niobate," *Nat. Commun.* **12**, 4453 (2021).
- ³⁸A. Wallraff, D. I. Schuster, A. Blais, L. Frunzio, R.-S. Huang, J. Majer, S. Kumar, S. M. Girvin, and R. J. Schoelkopf, "Strong coupling of a single photon to a superconducting qubit using circuit quantum electrodynamics," *Nature* **431**, 162–167 (2004).
- ³⁹S. A. Lynch, C. Hodges, S. Mandal, W. Langbein, R. P. Singh, L. A. P. Gallagher, J. D. Pritchett, D. Pizzey, J. P. Rogers, C. S. Adams, and M. P. A. Jones, "Rydberg excitons in synthetic cuprous oxide Cu₂O," *Phys. Rev. Mater.* **5**, 084602 (2021).
- ⁴⁰J. DeLange, K. Barua, A. S. Paul, H. Ohadi, V. Zwiller, S. Steinhauer, and H. Alaiean, "Highly-excited Rydberg excitons in synthetic thin-film cuprous oxide," *Sci. Rep.* **13**, 16881 (2023).
- ⁴¹J. Heckötter, B. Panda, K. Brägelmann, M. Harati, and M. Aßmann, "Neutralization of impurities by continuous-wave excitation of high-*n* Rydberg excitons," *Phys. Rev. B* **108**, 235212 (2023).
- ⁴²M. Khazali, K. Heshami, and C. Simon, "Single-photon source based on Rydberg exciton blockade," *J. Phys. B: At., Mol. Opt. Phys.* **50**, 215301 (2017).
- ⁴³J. Heckötter, V. Walther, S. Scheel, M. Bayer, T. Pohl, and M. Aßmann, "Asymmetric Rydberg blockade of giant excitons in cuprous oxide," *Nat. Commun.* **12**, 3556 (2021).

⁴⁴C. Morin, J. Tignon, J. Mangeney, S. Dhillon, G. Czajkowski, K. Karpiński, S. Zielińska-Raczyńska, D. Ziemkiewicz, and T. Boulier, “Self-Kerr effect across the yellow Rydberg series of excitons in Cu_2O ,” *Phys. Rev. Lett.* **129**, 137401 (2022).

⁴⁵V. Walther and A. S. Sørensen, “Quantum light from lossy semiconductor Rydberg excitons,” *Phys. Rev. Lett.* **131**, 033607 (2023).

⁴⁶J. Pritchett, “Microwave induced optical nonlinearities in cuprous oxide,” Ph.D. thesis, Durham University, 2023.

⁴⁷V. Walther, S. O. Krüger, S. Scheel, and T. Pohl, “Interactions between Rydberg excitons in Cu_2O ,” *Phys. Rev. B* **98**, 165201 (2018).

⁴⁸S. O. Krüger, H. Stolz, and S. Scheel, “Interaction of charged impurities and Rydberg excitons in cuprous oxide,” *Phys. Rev. B* **101**, 235204 (2020).